

Scientific Report: The Systematics and Operational Studies (SOS) Apparatus as a testbed for nEDM@SNS experiment

written by V. Cianciolo¹, R. Golub^{2,3}, B.W. Filippone³, P. R. Huffman^{2,3}, K. Leung^{2,3}, E. Korobkina^{2,3}, C. Swank^{2,3,4} on behalf of nEDM@SNS collaboration

¹*Oak Ridge National Lab, TN, USA*

²*North Carolina State University, Raleigh, NC 27695, USA*

³*Triangle Universities Nuclear Laboratory, Durham, NC 27708, USA*

⁴*California Institute of Technology, Pasadena, CA 91125, USA*

I. INTRODUCTION

The nEDM experiment at the SNS (nEDM@SNS) [1] is the first measurement of the neutron EDM to directly measure the precession frequency of the neutron spin due to magnetic and electric fields. Previous measurements have inferred the precession frequency by measuring the residual polarization of neutrons after a long period of free precession. This difference provides independent information on potential unknown systematic uncertainties compared to previous and on-going measurements. It is precisely because nEDM@SNS is using a number of novel techniques, that it is essential to perform detailed studies of these techniques in order to optimize the statistical sensitivity and minimize the systematic uncertainty. While these studies can, and in some cases will, be done with the full-scale apparatus, the significant cost of operating the nEDM@SNS (including the significant down-time required to make small changes to the apparatus) drives us to consider alternative, cost-effective ways to perform some of these studies.

The nEDM@SNS apparatus is designed to maximize statistical sensitivity and minimize systematic uncertainty in extracting a neutron EDM signal. This mandates long neutron storage times as well as long neutron and ³He polarization times. These in turn mandate requiring highly uniform fields and high ³He polarization at a low concentration. The Systematics and Operational Studies Apparatus (SOSA) does not need this level of statistical sensitivity and systematic error reduction. Therefore, it can operate with less field uniformity and lower ³He polarization. This allows the SOSA to be a much more nimble device that can have a turn around time of a few weeks rather than months, which in turn will be much less expensive to operate.

We identify three major studies to be performed with the SOS apparatus:

- Detailed studies of neutron and ³He correlation functions to characterize key systematic uncertainties
- Optimization of simultaneous spin manipulation of polarized neutrons and ³He
- Identification of high-performance measurement cells

II. OVERVIEW OF THE SYSTEMATICS AND OPERATIONAL STUDIES (SOS) APPARATUS

A Systematics and Operational Studies (SOS) apparatus has been designed to perform measurements that require the presence of polarized ultracold neutrons (UCNs) and/or polarized ³He dissolved in superfluid helium near 400 mK. There will be magnetic fields for spin manipulation and two detection techniques: SQUIDs for ³He magnetization measurements, and scintillation light detection to monitor UCN density and the angle between the ³He and UCN spins. There is no need for electric fields.

The total volume of LHe in the SOS apparatus is about 5 liters and the turnaround time of the system (cooldown & warm up) is ~ 2 weeks (~ 4 -5 times shorter than nEDM@SNS). Polarized ³He will be injected and removed each cycle with a turnaround time of ~ 2 -3 hours (~ 10 times longer than nEDM@SNS). Thus, while the main nEDM@SNS apparatus is more effective in collecting high sensitivity data, the SOS apparatus is preferable for commissioning phase measurements that require frequent warm-up and opening for adjustments and, likely, many more cool-downs.

A simplified schematic of the SOS apparatus is shown in Fig. 1 with a more detailed description and figures found in Appendix 2. The cooling system is based on the use of an existing Dilution Refrigerator (DR) that has a cooling power of ~ 5 mW at 400 mK (see 2). Originally, DR had only one pump but we have added another one to increase the cooling power. The mixing chamber of the DR will be connected to the ^4He -buffer/ ^3He -evaporation cell, which in turn is linked to the measurement cell through 0.5” tubing filled with superfluid ^4He serving as a cooling link. During cooldown, the isotopically pure ^4He will be condensed into the buffer cell.

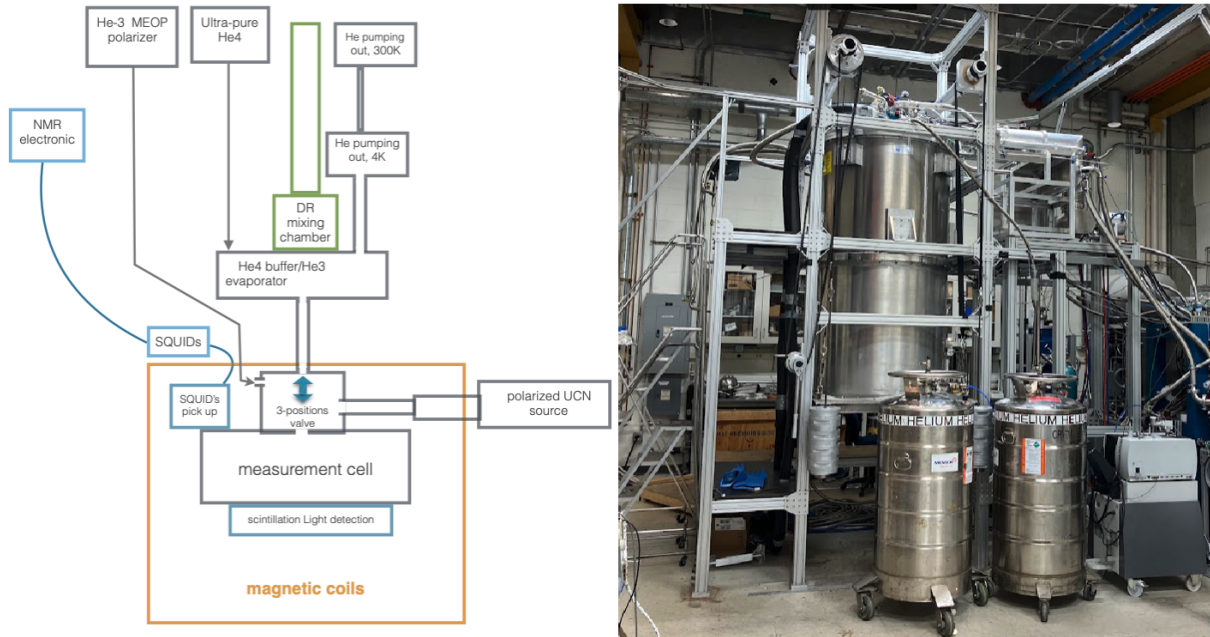


FIG. 1. Left - Simplified layout of the Systematics and Operational Studies (SOS) apparatus at PULSTAR. Note that in Phase I (studies with only polarized He-3) there will be no UCN guide and light collection system. Right - photo of the Phase I of the SOS apparatus at TUNL, Duke University

Isotopically clean ^3He will be polarized using the Metastability Exchange Optical Pumping (MEOP) technique for ~ 10 min at a pressure of a few mbar to achieve a ^3He polarization up to 70%. The required amount of ^3He atoms will be diluted to achieve the desired ^3He density in the cell, mixed with ^4He to ~ 500 mbar, and then injected to the measurement cell via cryopumping onto the liquid surface inside the apparatus. The ^3He will then transport into the measurement cell via diffusion.

Removal of depolarized ^3He from the measurement cell at the end of cycle will be done with the heat flush technique, which uses phonon flow (produced by heating the cell) to force ^3He into the evaporator cell. The ^3He vapor will be then pumped out by a charcoal adsorption pump at 4 K. The pump can be regenerated when saturated by heating and then pumping out with an external room temperature pumping system.

Neutrons will be delivered to the cell through the 3-position “vestibule” valve from an external UCN source. The current plan is to use the PULSTAR UCN source, which is now at the final stages of cryogenic commissioning. The back-up plan is to use the LANL UCN source.

The measurement cell will be made from PMMA as is the case for the nEDM@SNS experiment. The cell can be made identical to the nEDM cell or smaller for additional studies. The 3-position valve housing will have a flange identical to the nEDM cell to allow testing of the nEDM cells before assembling them into the nEDM apparatus. The 3-position valve will allow: (a) filling the measurement cell with polarized ^3He and UCN, (b) storing UCN and ^3He , and (c) connection of the measurement cell to the evaporator cell for removal of depolarized ^3He .

The neutron absorption cross section of ^3He is strongly dependent on the angle between the spins of the

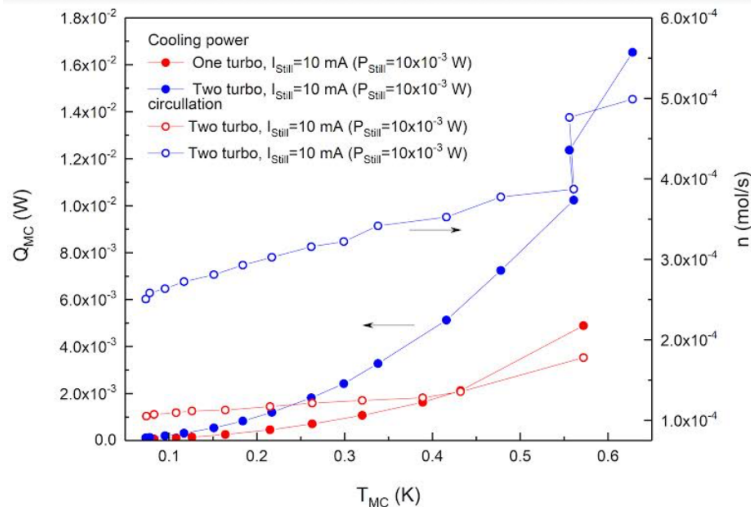


FIG. 2. Temperature dependence of Cooling power and He-3 circulation flows of the SOS Dilution Refrigerator. Solid circles - one pump, open circles - two pumps

neutron and ^3He : it is nearly zero when the spins are parallel and is at a maximum of 11 kilobarns at thermal neutron energies when the spins are anti-parallel. The angle between the neutron and ^3He spins can be monitored by the rate of $n\text{-}^3\text{He}$ capture resulting in scintillation light produced in the superfluid helium. To detect the light, we will use and test a prototype light collection system developed for the nEDM@SNS experiment. It will utilize wavelength shifting (WLS) fibers coupled to Silicon Photomultipliers (SiPMs) located at 77 K. The ^3He magnetization will be monitored by a SQUID magnetometry system using the latest design (e.g. the currently envisioned “4 pack” configuration) and its associated electronics for the nEDM experiment.

The magnetic fields required for spin related experiments will be produced by a magnetic coil package, designed in a similar way as the magnetic package of the nEDM@SNS experiment, but with less stringent field gradient requirements to reduce the size of the SOS apparatus coil package. This approach will allow us to study different procedures for spin manipulation and check if any hardware adjustments are required to the full-scale nEDM magnet package in advance to assembling of the main nEDM apparatus.

III. SCIENTIFIC PROGRAM OF MEASUREMENTS WITH SOS APPARATUS

The timeline of our studies are divided into two phases. In Phase I, the polarized ^3He injection and removal system, SQUID system, and magnetic field coils will be installed. This will allow measurements involving polarized ^3He (e.g. ^3He friendliness of cells and ^3He correlation studies). In Phase II, the apparatus will be coupled to a polarized ultracold neutron source and the light collection system installed. This will allow the rest of the measurement program (e.g. neutron friendliness of cells and simultaneous spin manipulation of the two species) to be performed.

A. Control of systematic effects via measurement of correlation functions

The leading systematic effect in the nEDM@SNS experiment is the false EDM produced by the interaction between the $\vec{E} \times \vec{v}/c$ motion-induced magnetic field and ever-present magnetic field gradients. The combination of these two fields produces time-dependent magnetic fields in the plane perpendicular to B_0 , and thus cause Bloch-Siegart precession frequency shifts that turn out to be linear in E (and flip sign with

the direction of E). This is often called the “geometric phase induced” frequency shift, but will be called the “linear-in- E ” shift here, and denoted by $\delta\omega$. The size of this shift depends on the geometry of the trap and the magnetic field gradients present. Furthermore, it also depends on a particle’s gyromagnetic ratio, velocity and trajectory, so that the size of $\delta\omega$ is different between the neutron and ${}^3\text{He}$. Therefore, this shift is generally not corrected for by the ${}^3\text{He}$ comagnetometer and will produce a false neutron EDM signal.

The philosophy of the measurement program described here is to measure the correlation functions of the ${}^3\text{He}$ and ultracold neutron motion via spin relaxation times (or frequency shifts) induced by the presence of known applied magnetic field gradients. The electric field is not required since it does not affect the neutron or ${}^3\text{He}$ motion. Once the correlation functions are determined, they can be used to predict and control the systematic error caused by the linear-in- E frequency shift and its associated false EDM effect. Indeed, for ${}^3\text{He}$ the size of $\delta\omega$ can be made minimal by an appropriately tuned superfluid helium temperature because the mean-free-path of ${}^3\text{He}$ diffusion, dominated by ${}^3\text{He}$ scattering off phonons in the superfluid, is strongly temperature dependent ($\propto T^{7.5}$). The ultracold neutron motion is unaffected by temperature since the phonon scattering time constant at 0.5 K is $\gtrsim 10,000$ s, and if they were to scatter, they would be lost since the typical energy gain is much larger than the storable UCN energy.

The variation of the B-field over the measurement cells can be characterized by the spectrum of the correlation function [2–4]:

$$S_{B_i B_i}(\omega_0) = \int_0^\infty \langle B_i(t) B_i(t + \tau) \rangle e^{-i\omega_0 \tau} d\tau, \quad (1)$$

where $\omega_0 = \gamma B_0$, B_i is the field along \hat{i} experienced by the particle, and $\langle \dots \rangle$ is the ensemble average.

With the holding field B_0 along the z -direction, the x -direction as the long, 40 cm axis of the cell, and the y -direction as the 10.2 cm dimension of the cell, the linear-in- E frequency shift $\delta\omega$ is written as:

$$\delta\omega = \frac{\gamma^2 E}{c^2} [\omega_0 \text{Im}(S_{B_x B_x}(\omega_0)) + \omega_0 \text{Im}(S_{B_y B_y}(\omega_0)) + \langle x B_x \rangle + \langle y B_y \rangle]. \quad (2)$$

A sensitive measurement of the correlation function allows for characterization and potentially subtraction of the linear-in- E shift. Therefore, a quantitative understanding of the behavior of the correlation functions for both ${}^3\text{He}$ and neutrons near the expected operating parameters is critical.

A quantitative characterization of the imaginary part of the correlation function allows for correction of $\delta\omega$. In fact the correlation functions can be accessed without an E -field by studying spin relaxation. For example in a constant applied magnetic gradient, $G_i = \partial B_i / \partial i$, the longitudinal relaxation is given by:

$$\frac{1}{T_{1,\text{gradient}}} = \frac{\gamma^2}{2} (G_x^2 \text{Re}[S_{xx}(\omega_0)] + G_y^2 \text{Re}[S_{yy}(\omega_0)]), \quad (3)$$

where, for example, $S_{xx}(\omega_0) = \int_0^\infty \langle x(t)x(t + \tau) \rangle e^{-i\omega_0 \tau} d\tau$.

The transverse relaxation for an applied gradient oscillating with frequency ω_{rf} is given by:

$$\frac{1}{T_{2,\text{rf gradient}}} = \frac{\gamma^2 G_{zx}^2}{2} \text{Re}[S_{xx}(\omega_{\text{rf}})], \quad (4)$$

where $G_{zx} = \partial B_z / \partial x$.

While Eqs. 3 and 4 are in terms of the real part, Eq. 2 depends on the imaginary part. In principle, the real and imaginary parts (cosine and sine transform) are related by the integral equations:

$$\text{Re}[S_{xx}(\omega)] = \int_0^\infty R_{xx}(\tau) \cos(\omega\tau) d\tau, \quad \text{and} \quad (5)$$

$$\text{Im}[S_{xx}(\omega)] = \int_0^\infty R_{xx}(\tau) \sin(\omega\tau) d\tau = \frac{1}{2\pi} \int_{-\infty}^\infty \frac{\text{Re}[S_{xx}(\omega')]}{\omega - \omega'} d\omega', \quad (6)$$

where

$$R_{xx}(\tau) = \langle x(t)x(t + \tau) \rangle \quad (7)$$

is the position auto-correlation function. Due to experimental constraints, it is not feasible to measure the correlation function across a sufficient range of ω to perform the integral in Eq. 6. However, the correlation function is determined from a conditional density $p(x, x_0, \tau)$, given by,

$$S_{xx}(\omega) = \int_{-\frac{\omega}{2}}^{\frac{\omega}{2}} \int_{-\frac{\omega}{2}}^{\frac{\omega}{2}} xx_0 p(x, x_0, \tau) e^{-i\omega\tau} dx dx_0 d\tau \quad (8)$$

so that we can fit the results to a model dependent conditional density that can be derived from both theory [5] and simulation [6]. The resulting conditional density will accurately predict the linear-in-E phase shift.

The typical gradients for measuring $T_{1,{}^3\text{He,gradient}}$ to determine the ${}^3\text{He}$ correlation function are $\sim 200 \mu\text{G cm}^{-1}$, producing $T_{1,{}^3\text{He,gradient}} \sim 100 \text{ s}$ (see Fig. 9 of Appendix 3). Due to the large polarized ${}^3\text{He}$ concentration $x_{\text{pol}3} \sim 10^{-7}$ that can be used without changing the motion of the ${}^3\text{He}$ (i.e. the ${}^3\text{He}$ mean-free-path remains dominated by scattering off phonons in the superfluid helium), reaching the required sensitivity can be easily achieved. The expected precision on the correlation function extracted from this technique in the worst-case is $\lesssim 10\%$, but will likely be much better after gaining experience on implementing the techniques. Measurements of $T_{1,gradient}$ to extract the correlation functions in small $\sim 1 \text{ in}^3$ cells and at different ${}^3\text{He}$ motion regimes (due to the high $x_{\text{pol}3}$ required for sufficient signal) have already been demonstrated in separate measurements [7].

Another technique we can consider is measuring the “ B^2 precession frequency shift” from gradients G_x and G_y that is given by:

$$\delta\omega_{B^2} = \frac{\gamma^2}{2} (G_x^2 \text{Im}[S_{xx}(\omega_0)] + G_y^2 \text{Im}[S_{yy}(\omega_0)]) . \quad (9)$$

We see that measuring $\delta\omega_{B^2}$ is attractive because it is a direct measure of the imaginary parts of $S_{ii}(\omega)$, which is required to predict $\delta\omega$ (see Eq. 2). To demonstrate the sensitivity of measuring $\delta\omega_{B^2}$ in the SOS apparatus, Fig. 3 shows the $\delta\omega_{B^2}$ shift by applying $G_x = 10 \mu\text{G cm}^{-1}$. This is compared in the plot with the frequency sensitivity δf of the SOS apparatus’s SQUID system assuming $T_{2,{}^3\text{He}} = 400 \text{ s}$ and a signal-to-noise ratio of SNR = 40. The size of the induced $\delta\omega_{B^2}$ is $\sim 100\times$ larger, and thus can be easily measured. This technique has the potential to be better than the T_1 measurements. However it has yet to be experimentally demonstrated; at the very least, it would provide a cross-check of the other techniques. Some of the systematic effects involved when determining $\delta\omega_{B^2}$ are discussed in Appendix 3.

So far we have only discussed measurements of the ${}^3\text{He}$ correlation function. To determine the neutron correlation functions, measurements of the spin relaxation times and $\delta\omega_{B^2}$ can also be performed. This can be done by using the n- ${}^3\text{He}$ capture scintillation light. Measurement of $T_{1,n}$ is discussed in Sec. III C. Measurement of $T_{2,n}$ can be done by measuring $T_{2,\text{tot}}$ from a free precession measurement. $T_{2,\text{tot}}^{-1} \approx T_{2,n,\text{gradient}}^{-1} + T_{2,{}^3\text{He,gradient}}^{-1}$ in the presence of sufficiently large applied field gradients, so $T_{2,n,\text{gradient}}$ can be deduced since $T_{2,{}^3\text{He,gradient}}$ is known from the SQUID measurements. The $\delta\omega_{B^2}$ shift of the neutron can also be determined with the free precession light signal, with approximate sensitivities given in Table II, which is of sufficient precision.

At this time it is not clear which of the three techniques (measuring $T_{1,gradient}$ or ω_{B^2} static gradients or measuring $T_{2,\text{rf gradient}}$ in RF gradients) is superior or what combination must be measured. Each contain different sensitivities and systematics. Further discussion of the correlation function measurements, measurement procedure, sensitivity can be found in Appendix 3.

B. Simultaneous neutron and ${}^3\text{He}$ spin manipulation

The nEDM@SNS experiment requires simultaneous manipulation of both the neutron and ${}^3\text{He}$ spins to carry out the experiment. This includes the $\pi/2$ pulse which rotates the spins from parallel to perpendicular

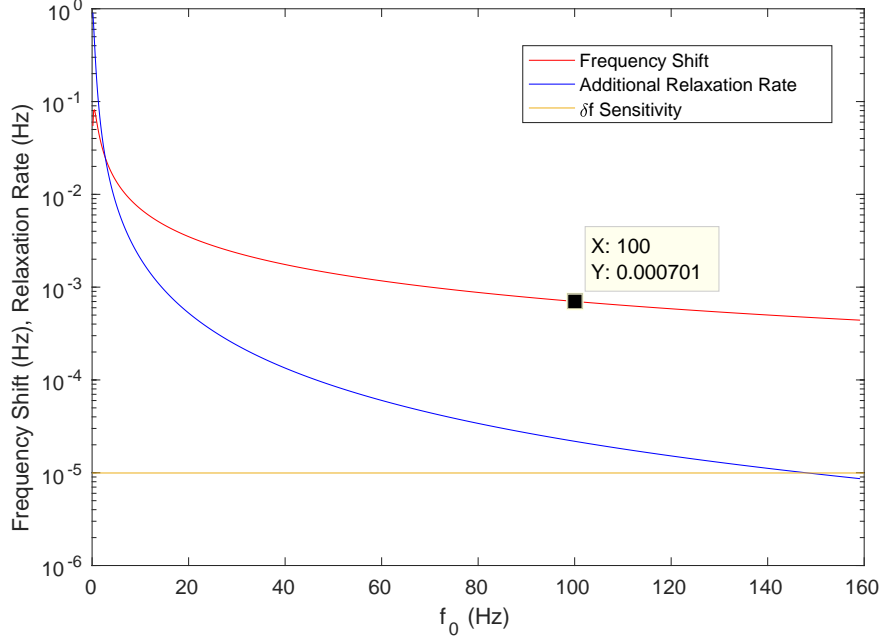


FIG. 3. The $\delta\omega_{B^2}$ frequency for ${}^3\text{He}$ in a $10\ \mu\text{G cm}^{-1}$ gradient along the x -direction (40 cm cell axis). The frequency sensitivity δf that is attainable with the SQUIDS in the SOS apparatus is also shown. $f_0 \approx 100$ Hz, corresponding to $B_0 \approx 30$ mG, is the operating frequency of the SOS apparatus and the nEDM@SNS experiment. For comparison, the additional contribution to the longitudinal relaxation of ${}^3\text{He}$ ($T_{1,{}^3\text{He,gradient}}$) due to the same gradient is also shown.

with respect to the applied B_0 field and the measurement technique utilizing critical spin dressing. Our sensitivity estimates to a neutron EDM of $\sim 5 \times 10^{-28}$ e·cm for the free precession mode, and $\sim 3 \times 10^{-28}$ e·cm for the dressed-spin mode that offers an independent measurement with different systematics, depend on our control of these processes. Inadequate control of our simultaneous spin manipulations will cause a worsening of the nEDM@SNS experiment from our stated sensitivities.

The $\pi/2$ spin rotation is, in principle, fairly straightforward. A short pulse of AC magnetic field with frequency close to the neutron precession frequency but at a fraction of the amplitude of B_0 is applied perpendicular to B_0 . At the end of the pulse both the neutron and ${}^3\text{He}$ are perpendicular to B_0 and begin to precess about B_0 , but with an initial angle, or phase ϕ_0 between the spins as described in Sec. 1. Without the ability to reproducibly set the initial phase to the level of 1 mrad (or 0.06°) for each measurement, our nEDM sensitivity would be negatively impacted. The uncertainty in the measured frequency $\sigma_{\nu_{\text{free}}}$ per free precession cycle will increase from $1.8\ \mu\text{Hz}$ to $2.8\ \mu\text{Hz}$, resulting in a corresponding worsening of our nEDM sensitivity.

The simultaneous $\pi/2$ pulse technique required to do this can be demonstrated and optimized (since there are many possible frequencies and AC B-field values that can be used) with the SOS apparatus. As shown in Table II, the 1σ fitted uncertainty in ϕ_0 from each free precession cycle will be as low as 0.6° . Therefore, by performing repeated measurements of ϕ_0 and by comparing if the population standard deviation is larger than the expected from fitting statistics alone, the initial stability of ϕ_0 can be deduced to $\sim 10\%$ from the $\sigma_{\phi_0} \approx 0.6^\circ$ from the fitting. This lets us reach the 0.06° precision goal.

In addition sufficient reduction and stability of the ${}^3\text{He}$ elevation angle after the $\pi/2$ pulse is required to reduce the systematic shift and the additional noise in the extracted ν_{free} caused by the pseudomagnetic effect produced by the n- ${}^3\text{He}$ spin-dependent scattering length difference.

If the ${}^3\text{He}$ spin has an elevation angle of 0.3° from the plane perpendicular to B_0 , the precession frequency shift from the pseudomagnetic field is $\sim 1.6\ \mu\text{Hz}$, around the same precision at which we can measure ν_{free} per free precession cycle in the nEDM@SNS experiment. This shift will on average be cancelled when

subtracting the difference between the two cells in the nEDM@SNS experiment. However, if insufficient control of the ^3He tipping causing a difference in the elevation angle between the two cells, noise will be introduced when taking the frequency difference and thus reduce the sensitivity to a neutron EDM in the nEDM@SNS experiment. For small angles, the size of the pseudomagnetic frequency shift is proportional to the tipping angle. Therefore, the ^3He elevation angle after tipping should be controlled to $\lesssim 0.03^\circ$ ($\lesssim 10\%$ of the fitting uncertainty of $1.8 \mu\text{Hz}$ per free precession measurement).

Fluctuations of the ^3He tipping angle of 0.03° produces a shift of only $0.16 \mu\text{Hz}$ if $x_{\text{pol}3} = 8 \times 10^{-11}$. However, if $x_{\text{pol}3} = 8 \times 10^{-10}$ is used in the SOS apparatus, then this produces a shift of $1.6 \mu\text{Hz}$. With $x_{\text{pol}3} = 8 \times 10^{-10}$, from Table II, the noise from fitting statistics only $\sigma_{\nu_{\text{free}}} = 50 \mu\text{Hz}$ per free precession measurement. We will thus be able to determine additional contribution to the noise to $\sim 10\%$ of this by repeated measurements (as described for the ϕ_0 measurements). This corresponds to ^3He tipping angle fluctuations of $\sim 0.1^\circ$. This is somewhat larger than what's required but performing this measurement in the SOS apparatus will identify promising ^3He tipping pulse techniques and ways to operate the electronics for the nEDM@SNS experiment.

Use of the spin dressing technique can also provide improved sensitivity to the neutron EDM by fixing the angle between the neutron and ^3He spins compared to the free precession. This effectively uses the capture events more efficiently. Best sensitivity is achieved, with minimal additional noise from the pseudo-magnetic field effect, by modulating the neutron- ^3He angle from e.g. $+\phi_0$ to $-\phi_0$. This introduces additional control parameters in the technique. Thus, while the spin dressing technique using this "critical" dressing is quite promising, the critical' dressing condition has not been studied experimentally and includes many variables the should be optimized, including dressing field, dressing frequency, modulation frequency, modulation waveform, ϕ_0 , etc..

Exploring this phase space experimentally will certainly take some time and may well include adjustments to the hardware (i.e. multiple cooldowns) such as additional AC shim coils, optimizing pick-up loops for AC B-field feedback, etc. Optimizing this technique could well take many months and multiple cooldowns to converge. Performing this optimization with the SOS Apparatus will almost certainly reduce the number of cooldowns as well as operation time required for the main apparatus as the critical dressing parameter space is studied.

C. Cell testing

Measurements of the ^3He depolarization rate and UCN loss probability on the measurement cell walls form the basis of the cell testing program. We currently do not have a good estimate for the probability to produce a good cell. We also do not have a good estimate for how frequently we'll need to change cells (e.g., due to spark damage, formation of a leak, or magnetic contamination). But we do know that every bad cell identified by the SOS apparatus – and therefore not installed – will save a cooldown cycle.

Loss of ultracold neutrons and depolarization of neutrons and ^3He cause a reduction in statistical sensitivity. Plots showing how reductions in τ_{tot} and $T_{2,\text{tot}}$ affect the scintillation light signal for free precession measurements are shown in Fig. 4. In these examples, a reduction of τ_{tot} from the nEDM@SNS design goal of 2000 s to 600 s, and the design goal $T_{2,\text{tot}}$ from 10,000 s to 1000 s, both cause a reduction in sensitivity to a neutron EDM in the final nEDM@SNS experiment by a factor of ~ 2 .

Effects that can cause increases in UCN loss and neutron and ^3He depolarization include:

- coating imperfections at the cell walls;
- gluing imperfections at the cell inner corners;
- contamination (nuclear or magnetic) inside the cell;
- coating micro-roughness.

The current active measurement cell and UCN storage program so far has focused on reducing neutron losses only. Ultracold neutron storage measurements have been performed in vacuum down to ~ 15 K. While studies have been done on ^3He depolarization on small-scale coated cells ($\sim 1'' \times 1'' \times 1''$) by our

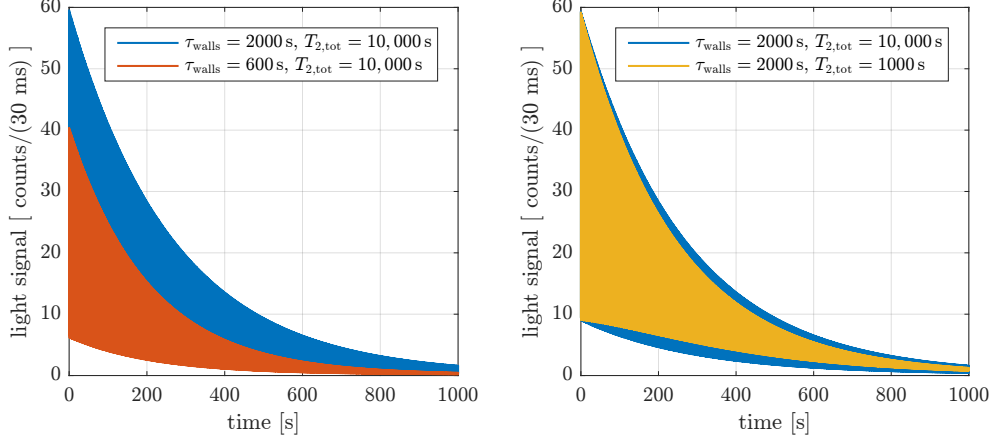


FIG. 4. Example of how ultracold neutron losses and depolarization of neutron and ^3He affects the scintillation light signal from free precession measurement and reduces the statistical sensitivity on the nEDM@SNS experiment. The lines shown are those from fitting Monte Carlo generated light signals using Eq. 10. The oscillations at $\omega_{\text{free}} \approx 100$ Hz can't be resolved visually in these plots.

collaboration at close to our operating conditions (~ 0.4 K and $B_0 \sim 7$ G), they have yet to be done on full-sized cells. Neutron depolarization measurements have also not been performed on our coatings.

The SOS apparatus will be able to measure the loss and depolarization properties of full-sized measurement cells at the final operating conditions (final temperature in superfluid helium and close to final magnetic fields) in a single apparatus. Use of full-sized, final cells are important since the production process produces different coating qualities and possibility different contamination. New magnetic effects might appear at the final temperatures as well.

It should be emphasized that after the cell properties have been verified in the SOS apparatus, the same cells will be installed in the full nEDM apparatus, significantly reducing the risk and time costs of installing a poor quality cell. Contamination on the inside of a cell is most likely to occur before (e.g. already in the coating solution) and during cell production (e.g. airborne dust or magnetic particles) due to the large surface area and exposure time. From previous UCN storage measurements, we have demonstrated that reinstalling the cell after exposure to air and repeated cooldowns does not degrade the neutron storage properties of the cell.

The τ_{tot} of a cell can be measured by using the exponentially decaying scintillation light from β -decay without ^3He . A day of measurements on the SOS apparatus will produce $\sigma_{\tau_{\text{tot}}} \lesssim 6$ s for a UCN density $\rho_{\text{UCN}} = 30 \text{ UCN cm}^{-3}$, corresponding to $\sigma_{\tau_{\text{walls}}} \lesssim 20$ s, which will be of sufficient accuracy.

The wall contributions to $T_{2,\text{tot}}$ (see Eq. 12) are given by $T_{2,\text{n,walls}} = 2T_{1,\text{n,walls}}$ and $T_{2,^3\text{He,walls}} = 2T_{1,^3\text{He,walls}}$. Therefore, it is sufficient to determine the longitudinal relaxation times $T_{1,\text{walls}}$. Generally, one measures $1/T_{1,\text{tot}} = 1/T_{1,\text{walls}} + 1/T_{1,\text{gradient}}$. However, in the SOS apparatus' magnetic field gradients of ~ 500 nG/cm the expected $T_{1,\text{gradient}} \gtrsim 10^6$ sec for both ^3He and neutrons. Therefore, $T_{1,^3\text{He,tot}} \approx T_{1,^3\text{He,walls}}$ and $T_{1,\text{n,tot}} \approx T_{1,\text{n,walls}}$, which avoids the need of separating out the two longitudinal relaxation contributions.

$T_{1,^3\text{He,walls}}$ can be measured with the SQUID magnetometer using a common NMR technique where the ^3He spin is repeatedly tipped by a small angle ($\sim \pi/4$) from B_0 with long known time delays in between (e.g. ~ 1000 sec). Due to the large polarized ^3He concentration that can be used for these measurements in the SOS apparatus, the desirable precision can be easily obtained.

To determine $T_{1,\text{n,walls}}$, the scintillation light signal when leaving both the neutron and ^3He spins aligned with B_0 can be used. Knowledge of τ_{tot} and $T_{1,^3\text{He,walls}}$ from the two previous measurements can then be used to extract $T_{1,\text{n,walls}}$. This is described in more details in Appendix 4.

TABLE I. Summary of experimental design differences between the full nEDM@SNS experiment and the SOS apparatus at PULSTAR

	<i>nEDM@SNS</i>	<i>SOS apparatus</i>
measurement cell	2× cells	1× full-sized cell, designed so can be installed in nEDM
high voltage	direct-feed and then Cavallo	none
0.4 K superfluid He	~ 1000 L	~ 5 L
ultracold neutrons	UCN production inside of cell with the FNPB cold neutron beam	UCNs fed in from external UCN source
polarized ^3He	ABS system: $x_3 \sim 10^{-10}$ and $P_3 \sim 98\%$	MEOP system: x_3 can reach 10^{-7} with $P_3 \sim 70\%$
magnetic field gradients	< 100 nG/cm or $< 3 \times 10^{-6}$ cm $^{-1}$ for $T_{\text{gradient},^3\text{He}} > 10,000$ sec	< 500 nG/cm or $< 1.5 \times 10^{-5}$ cm $^{-1}$ for $T_{\text{gradient},^3\text{He}} > 400$ sec
measurement cycle rate	30×/day (dead time = 400 s, 24 hours/day)	3×/day (dead time = 2 hrs, 9 hours/day)

IV. EXPERIMENTAL DESIGN DIFFERENCES BETWEEN NEDM@SNS AND SOS APPARATUS

The experimental design differences between the SOS apparatus and the nEDM@SNS experiment summarized in this section are what allow the size, complexity and turnaround times of the former to be reduced relative to the latter. The SOS apparatus will have a single full-sized measurement cell filled with isotopically pure superfluid helium at the final operating temperature of ~ 0.4 K. The cell hole sealing geometry and interface to the vestibule of the 3-position valve of the SOS is designed so that it can be used with the V1-valve system of the nEDM experiment. Therefore, the cells tested in the SOS apparatus will be fully transferrable to nEDM after testing. Indeed, this is one of the main goals of the measurement program described in Sec. III C.

There will be no high voltage system in the SOS apparatus. However, the systematic error resulting from the interaction of the motional ($\vec{E} \times \vec{v}/c$) magnetic field with stray magnetic field gradients (often called the “geometric phase” induced false EDM effect) can still be predicted using the SOS apparatus. As described in more details in Sec. III A, this is done by studying the motion of the UCNs and ^3He via characterization of the correlation functions. These studies do not require an electric field. Furthermore, a dummy ground electrode can be installed in the SOS apparatus for instrumentation tests of the SQUID system.

The ultracold neutrons used in the SOS apparatus will be loaded into the measurement cell from an external source rather than produced *in-situ* with the FNPB cold neutron beam for nEDM@SNS. This results in absence of any activation background as well as a reduction in the initial UCN number of around an order of magnitude. The setup can also be upgraded to run at a cold neutron beam.

A MEOP polarized ^3He source at room temperature will be used in the SOS apparatus rather than the cryogenic atomic beam source (ABS) which will be used in the nEDM@SNS apparatus. The MEOP system compared to the ABS can produce 2-3 orders of magnitude more polarized ^3He atoms with the trade-off of a reduced polarization ($P_3 \sim 98\%$ vs. 70%). A higher number of polarized ^3He atoms will make measurements using only ^3He and SQUIDS more easily performed and with better statistics.

The trade-off with the MEOP system’s lower P_3 is that achieving the same SQUID ^3He signal strength, the n- ^3He absorption loss will be higher. For example, in the nEDM@SNS experiment the optimal is $x_{\text{pol}3} = 8 \times 10^{-11}$ for extracting the oscillating frequency from the free precession light signal (see Sec. 1). If the noise in the SQUIDS of the SOS apparatus are the same as in the nEDM experiment, then to have the same signal-to-noise ratio the neutron- ^3He absorption time constant τ_3 will decrease from 500 s to 350 s (see Eq. 11). This shortens the useful observation time with ultracold neutrons in the SOS apparatus.

The magnetic field homogeneity that can be achieved in the SOS apparatus is reduced due to the reduced

available space and size compared to nEDM@SNS. However, the magnetic field requirements in the SOS apparatus are reduced because of the shorter observation time caused by the reduced P_3 discussed above. The transverse relaxation due to magnetic field gradients $T_{2,\text{gradients}}$ is proportional to the square of the linear gradients in the cell (e.g. see Eq. 2). The specified $T_{2,\text{gradients}}$ required in the SOS apparatus decreases to ~ 400 sec compared with $\sim 10,000$ sec in SNS@nEDM (e.g. $\sim 5\times$ poorer gradients).

An overview of these design differences is found in Table I. In summary, the SOS apparatus operates in a different part of experimental parameter phase space, with less required field uniformity and lower ^3He polarization (but with the possibility of much higher concentrations).

Appendices

Appendix 1 UNCERTAINTIES OF EXPERIMENTAL EXTRACTABLE PARAMETERS

To aid the discussion of the SOS measurement program and to show that it can be successfully achieved, a more quantitative discussion in terms of the uncertainties of experimental extractable parameters from the free precession mode light signal is described.

To illustrate the impact on the parameter uncertainties for the difference in designs, the light signal expected from the free precession measurements is simulated. For this case the number of detected scintillation light events y_i in a time bin with width Δt at time t_i during a free precession mode measurement is given by:

$$\frac{y(t_i)}{\Delta t} = I_0 e^{-t_i/\tau_{\text{tot}}} \left[1 - F e^{-t_i/T_{2,\text{tot}}} \cos(\omega_{\text{free}} t_i + \phi_0) \right] + R_{\text{BG}}, \quad (10)$$

where

$$I_0 = N_0 \left(\frac{\epsilon_\beta}{\tau_\beta} + \frac{\epsilon_3}{\tau_3} \right), \quad F = \frac{\epsilon_3 P_3 P_n}{\tau_3 \left(\frac{\epsilon_\beta}{\tau_\beta} + \frac{\epsilon_3}{\tau_3} \right)} \quad \text{and} \quad \tau_3 = \frac{2}{n v_\sigma \sigma_{\uparrow\downarrow}(v_\sigma) x_3}. \quad (11)$$

N_0 is the initial number of neutrons in the cell, ϵ_β is the detection efficiency for neutron β -decay ($n \rightarrow p + e + \bar{\nu}_e$) events, τ_β is the neutron β -decay mean lifetime of ~ 880 s, ϵ_3 is the detection efficiency of a n - ^3He capture event, τ_3 is the time-averaged n - ^3He capture rate determined by the amount of polarized ^3He loaded into the cell (n is the helium number density, $\sigma_{\uparrow\downarrow}(v_\sigma)$ is the cross-section of n - ^3He capture in the singlet state at the velocity v_σ , which for $v_\sigma = 2200 \text{ m s}^{-1}$, $\sigma_{\uparrow\downarrow} = 11 \text{ kb}$), P_3 and P_n are the initial ^3He and neutron polarizations, ω_{free} is the angular beating frequency between the ^3He and neutron spins ($\omega_{\text{free}} = 2\pi\nu_{\text{free}} = \gamma_3 B_0 - \gamma_n B_0$), ϕ_0 is the initial phase, and R_{BG} is the ambient background rate.

The contribution from losses and depolarization enter into Eq. 10 through the total neutron storage time τ_{tot} and the total transverse polarization relaxation time $T_{2,\text{tot}}$ given by:

$$\frac{1}{\tau_{\text{tot}}} = \frac{1}{\tau_3} + \frac{1}{\tau_\beta} + \frac{1}{\tau_{\text{wall}}} \quad \text{and} \quad \frac{1}{T_{2,\text{tot}}} = \frac{1}{T_{2,\text{n},\text{wall}}} + \frac{1}{T_{2,\text{n},\text{gradient}}} + \frac{1}{T_{2,^3\text{He},\text{wall}}} + \frac{1}{T_{2,^3\text{He},\text{gradient}}}, \quad (12)$$

where the ‘‘wall’’ subscripts are for contributions from the walls of the cell and the ‘‘gradient’’ subscripts in the expression for Eq. (12) refer to depolarization caused by magnetic field gradients. The wall contributions will be the same between SOS and nEDM (since the same cell that will be used) whereas the gradient contributions will be different (because of the different magnetic field coil and shielding).

The simulated light signal from a free precession measurement in the SOS apparatus is shown in Fig. 5. From fitting this data using an iterative re-weighted least squares fitting algorithm, the 1σ uncertainty in extracting the key parameters, $\sigma_{\tau_{\text{tot}}}$, $\sigma_{\nu_{\text{free}}}$ and σ_{ϕ_0} (leaving all these parameters free in the fit), are shown in Table II. Note that these uncertainties assume that ϕ_0 is left as a free parameter in the fit (see Sec. III B

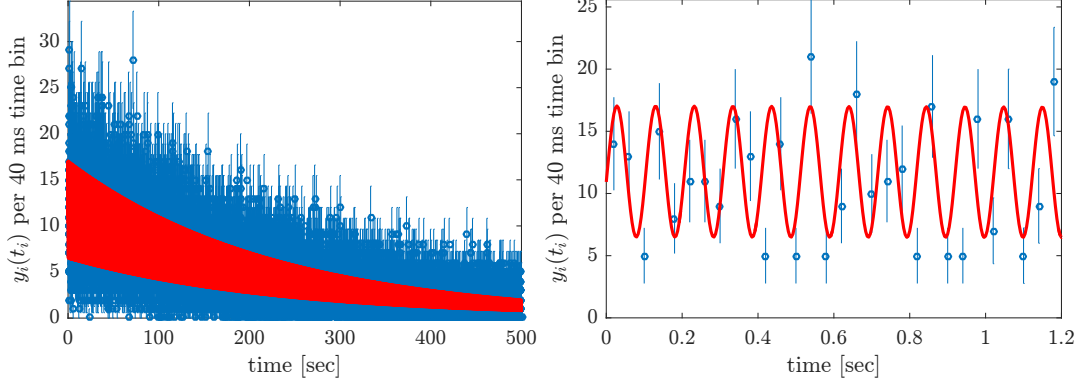


FIG. 5. The simulated scintillation light signal expected from the Systematics and Operational Studies apparatus during a free precession measurement. The red solid line is a fit to the binned data points. Shown on the right is a zoomed in view of the plot on the left.

for a discussion of reducing this uncertainty).

TABLE II. Uncertainties in the extracted parameters in the SOS apparatus per free precession cycle assuming: $P_n = 0.98$, $\tau_{\text{walls}} = 2000$ s, $\epsilon_3 = 0.93$, $\epsilon_\beta = 0.50$, $T_{2,\text{tot}} = 400$ sec, and $R_{\text{BG}} = 5$ Hz. The UCN density ρ_{UCN} and ^3He polarization P_3 are varied to see its impact. The effects of deliberately increasing $x_{\text{pol}3}$, which is possible due to the MEOP source, are also shown.

$T_{2,\text{tot}}$	ρ_{UCN}	P_3	$x_{\text{pol}3}$	τ_3	$\sigma_{\tau_{\text{tot}}}$	$\sigma_{\nu_{\text{free}}}$	σ_{ϕ_0}
400 s	10 cm^{-3}	0.5	8×10^{-11}	250 s	2 s	60 μHz	2.5°
			8×10^{-10}	25 s	0.2 s	150 μHz	1.6°
		0.7	8×10^{-11}	350 s	3 s	40 μHz	2.1°
	30 cm^{-3}	0.5	8×10^{-10}	35 s	0.2 s	80 μHz	1.1°
			8×10^{-11}	250 s	1 s	30 μHz	1.4°
		0.7	8×10^{-10}	350 s	1 s	20 μHz	1.1°
			8×10^{-9}	3.5 s	0.03 s	450 μHz	0.6°

The polarized ^3He concentration is scanned to illustrate the usefulness of having access to a wide range of $x_{\text{pol}3}$. In measurements where extraction of the neutron precession frequency is important, a low $x_{\text{pol}3} \sim 10^{-10}$ will be most useful. When extraction of the initial phase ϕ_0 is important, an intermediate $x_{\text{pol}3} \sim 10^{-9}$ will be most useful. Finally, when access to the polarized ^3He precession frequency or signal strength needs to be enhanced, operation with $x_{\text{pol}3} \sim 10^{-8}$ to 10^{-7} will be most useful. For $x_{\text{pol}3} \lesssim 10^{-7}$ the mean-free-path of the ^3He remains essentially unchanged since it is still in the regime where scattering with phonons in the superfluid helium dominates.

Appendix 2 DETAILED DESCRIPTION OF APPARATUS

A schematic of the experimental setup is shown in Fig. 6. Isotopically pure ^4He is inputted and condensed via the ^4He fill capillary to fill the ~ 5 L total volume of: the measurement cell; the “vestibule”, our name for the housing of a 3-position valve system; the “buffer volume”, a ~ 5 in diameter volume thermally connected to the mixing chamber (MC) of the dilution refrigeration (DR) using sinter as heat exchanger.

The vestibule connects the cell hole to the polarized ^3He input capillary, the ultracold neutron (UCN) guide, and the ^3He removal line (which also acts as the thermal link with the MC). With the 3-position

vestibule valve in the left-hand most position in Fig. 6, polarized UCNs and polarized ^3He can be loaded into the measurement cell. Then moving the vestibule valve to the right-hand most position, the UCNs and ^3He are confined in the cell for the measurements. The inner walls and the valve piston will be coated with deuterated plastic for good UCN reflection and low ^3He depolarization losses. The measurement cell will also be coated with deuterated plastic but with a deuterated fluorescent dye added for converting the superfluid helium scintillation light peaked at 80 nm to the blue region. At the end of a measurement, the vestibule valve is moved to the center position to allow the depolarized ^3He to be removed via the ^3He removal line.

Inside the inner vacuum chamber (IVC) below the height of the buffer volume, the components will be made from only plastics and composite materials to avoid magnetic inhomogeneities, as well as reducing RF-induced eddy current heating. The outer walls and thermal shields of the cryostat are made with aluminum and other non-magnetic materials as much as possible also. A 2-stage Gifford McMahon cryocooler (see Fig. 7) will be used for initial cooldown and to reduce cryogen consumption, but can be turned off during measurement to reduce magnetic and vibrational noise.

The UCNs from the external source will be polarized outside of the SOS apparatus. Our apparatus is envisioned to be used at the PULSTAR UCN source, which has been calculated to provide a density of 30 UCN cm^{-3} (unpolarized) at the source exit for the reactor operating at 1 MW, with there being a planned upgrade to 2 MW. To maintain neutron polarization non-depolarizing coatings of the UCN guides will be used. Inside the apparatus, the guide will transition from room temperature to the vestibule (see Fig. 8). There will be a thin-foil 4K window and a 45° bend section just before the vestibule to reduce radiation heating. There will be a thin-foil at the UCN guide entrance to the vestibule for containing the superfluid helium. Biaxially oriented polypropylene 0.0013 in thick has been tested to be superfluid tight and can withstand more than 1 bar pressure differential when cold. This thin foil with its near zero neutron optical potential will have a low UCN transmission loss.

The source of polarized ^3He will be a Metastable Exchange Optical Pumping (MEOP) system located above the cryostat connected to the polarized ^3He input capillary. A key difference between the SOS apparatus is the higher density of polarized ^3He that can be achieved in the cell compared with the atomic beam source (ABS) of the SNS nEDM experiment. The latter is optimized for $x_{\text{pol}3} \sim 10^{-10}$, equivalent to $\sim 10^{12} \text{ cm}^{-3}$ density in the cell. The SOS apparatus' MEOP system will produce $\sim 70\%$ polarized ^3He of ~ 1 Torr gas at room temperature ($\sim 3 \times 10^{16} \text{ cm}^{-3}$ density) in a volume $\sim 5\%$ relative to the superfluid volume in the SOS apparatus. Therefore, even after injection of the ^3He , many orders of magnitude higher polarized ^3He density can be loaded into the cell compared to the ABS system. A pre-holding volume will be used to control how much ^3He is injected. Of course, the trade-off is a lower polarization. A thin 2 mm tube made from glass and kapton thermally anchored at appropriate places and passing through the 4 K LHe bath will be used to reduce the heat load to the system during injection.

After a measurement, the ^3He from the cell will be removed via the ^3He removal line. When the vestibule valve is open the ^3He in the cell will diffuse up to the buffer volume until the ^3He density is constant. The liquid surface in the buffer volume will serve as an evaporator. The buffer volume is connected to a charcoal adsorption pump (CP), with a superfluid film suppression system (e.g. a film burner and film pinner), so that mostly gaseous helium from the buffer volume is pumped by the CP. The CP is a sealed volume containing ~ 1 kg of activated charcoal that is cooled with a thermal link to the 4 K LHe bath.

In equilibrium, the ratio of the ^3He density in the vapor just above the liquid in the buffer volume and the density of the ^3He dissolved in the superfluid just below the liquid level is given by: $n_{^3\text{He gas}}/n_{^3\text{He liquid}} \approx 2.4^{-3/2} e^{-(2.8 \text{ K})/T}$, where $n_{^3\text{He liquid}} = x_3 \times (2.2 \times 10^{22} \text{ cm}^{-3})$. And the partial pressure of ^3He in the gas is given by $P_{^3\text{He}} = n_{^3\text{He gas}} k_B T$.

The removal rate of ^3He is $\dot{Q}_{^3\text{He}} = P_{^3\text{He}} S$, where S is the pumping speed of the combined CP and conductance of the piping connecting the buffer volume to the CP. For our geometry, the pumping speed is dominated by the restriction of the piping. Therefore, if the temperature of the evaporator is increased from our nominal 0.4 K, $\dot{Q}_{^3\text{He}}$ will also increase; for example from 0.4 K to 0.5 K, $\dot{Q}_{^3\text{He}}$ increases by a factor of ~ 5 . This neglects the further increase due to the increase in conductance in the molecular regime $C \propto T^{1/2}$.

The capacity of the CP for helium at 4.2 K, assuming a pressure of 10^{-7} mbar, is 10 mol kg^{-1} . The amount of ^3He in the system if $x_3 \sim 10^{-10}$ is used is $\sim 10^{-8}$ mol. Thus, the CP has enormous capacity compared simply the amount of ^3He required to be removed. However, a much larger amount of evaporated ^4He will get adsorbed during the ^3He removal cycle. The partial pressure of ^4He , given by the vapor pressure, is

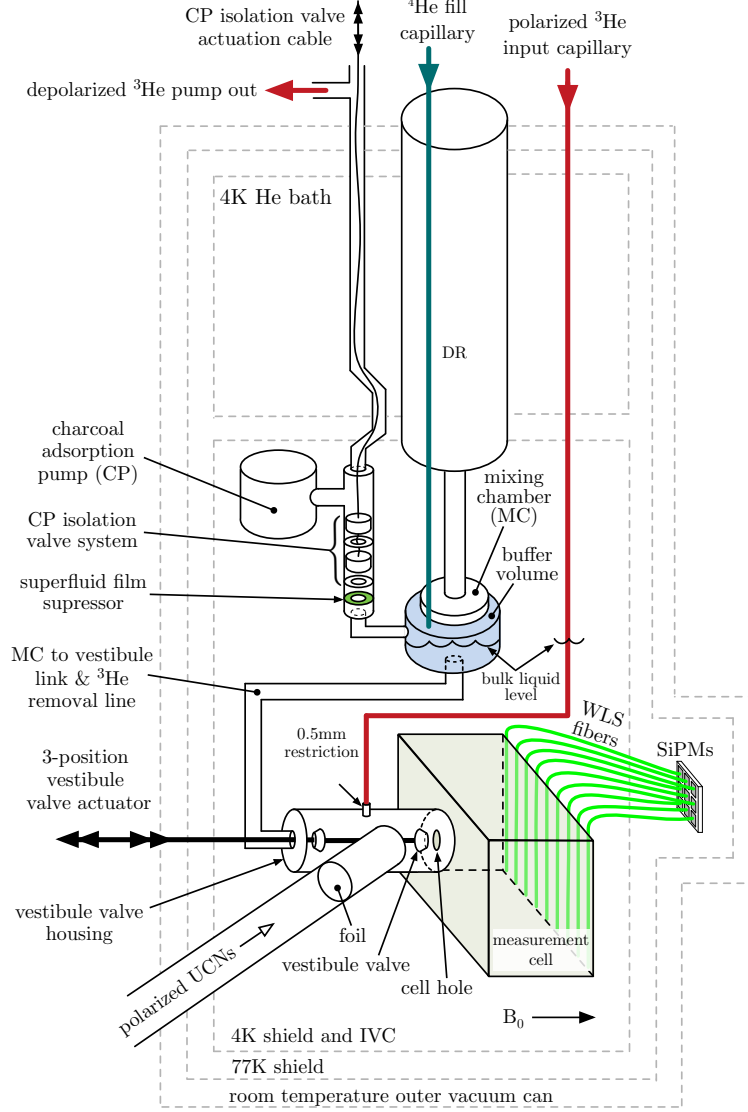


FIG. 6. Schematic of the SOS apparatus in Phase II. The magnetic coils, SQUID magnetometers and pick-up loops are not shown and many components are shown simplified. CAD drawings of the apparatus are in Figs. 7 and 8.

$P_{4\text{He}} \approx (680 \text{ mbar}) \times e^{-(8.6 \text{ K})/T}$, so the ratio of the partial pressures:

$$\frac{P_{4\text{He gas}}}{P_{3\text{He gas}}} \approx \frac{(0.35 \text{ K})}{x_3 T} e^{-(6.1 \text{ K})/T} \quad (13)$$

Therefore, if a higher T is used in the evaporator, more ^4He will be evaporated and be adsorbed by the CP. The optimal operating conditions will be depend on balancing between these effects. To further reduce ^4He from saturating the CP pump, a superfluid film suppressor and pinner will be used.

If the temperature in the evaporator needs to be raised during evaporation, it will be advantageous to raise the temperature by applying a heat load ($\sim 1 - 2 \text{ mW}$) using a heater at the measurement cell. By allowing phonons to flow from the measurement cell to the buffer volume, an added heat flush effect will be

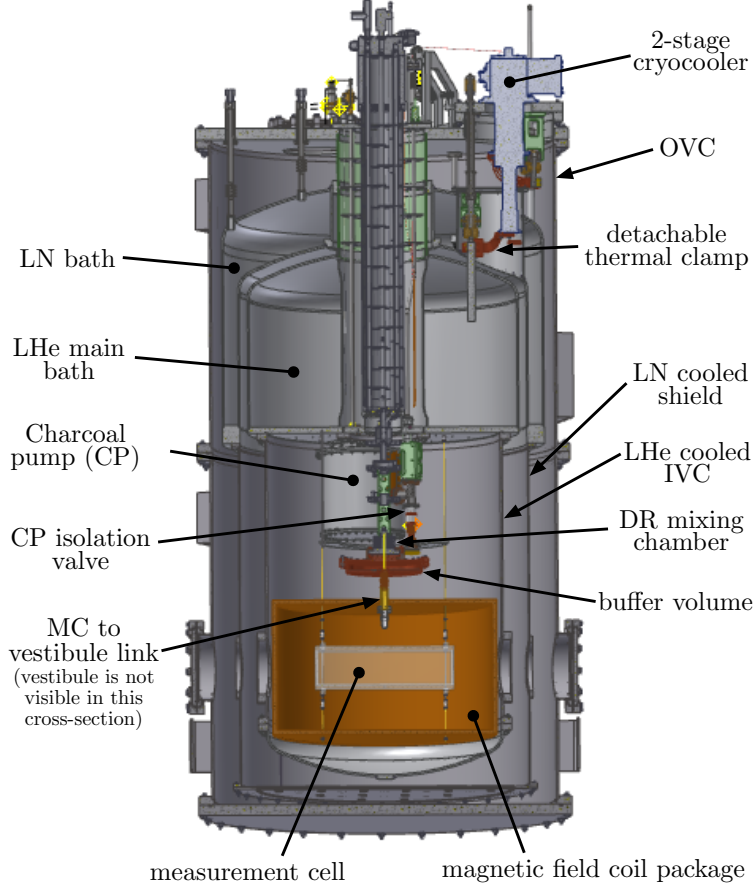


FIG. 7. 3D model of the apparatus. Shown as a vertical slice coincident on long central axis of the measurement cell. The WLS fibers, SiPMs and MEOP ^3He system are not shown here. The magnetic field coil package is shown schematically only.

applied on the ^3He and increase the density of ^3He in the buffer volume, thus further speeding up the ^3He removal time. With a buffer volume of ~ 0.2 L, the x_3 at the evaporator will be increased by $\gtrsim 10$ times, reducing the required evaporation time by a similar factor. The ^3He removal process is expected to take $\lesssim 3$ hours after, which the superfluid helium will be cooled back down to the nominal 0.4 K in preparation for the next measurement.

The ^3He removal system is designed so that it can be purged while the cryostat remains cold. For this procedure, the CP isolation valve is closed and the CP pump heated up with the thermal link between it and the 4 K LHe bath switched off. The desorbed ^3He and ^4He is then pumped out to room temperature. Due to the long pipe and small diameter, this process is expected to take a day or so to completely purge the charcoal.

During measurement, signals from the spin-dependent $n + ^3\text{He}$ capture events provides information on the neutron spin. After a $n + ^3\text{He} \rightarrow p + ^3\text{H}$ event, the 764 keV of kinetic energy will produce $\sim 6,400$ EUV scintillation photons in the superfluid helium peaked at 80 nm. These EUV photons will be down-converted to blue photons by the deuterated tetraphenyl butadiene (dTPB) doped dPS coating on the inner surface of the measurement cell. These blue photons are further down-converted into green photons at the core of 1.5 mm diameter wavelength shifting (WLS) fibers coupled to the outer walls of the cell. These fibers guide out the green photons to silicon photomultipliers (SiPMs) detectors situated in a volume at ~ 100 K, with an optical break at the IVC. The fibers will be coupled to one wall of the cell. There will also be dielectric

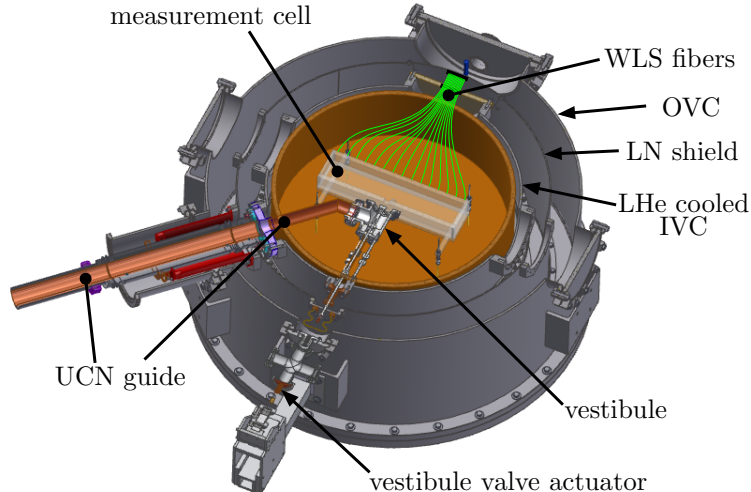


FIG. 8. 3D model of the apparatus. Shown as a horizontal slice coincident on the long central axis of the measurement cell. The WLS, SiPMs and magnetic field coil package are shown schematically only.

reflecting film on the outside of the fibers and around the cell (not shown in the figures) to increase the light capture efficiency. An estimate of ~ 30 photo-electrons (PEs) will be produced by the SiPMs, taking into account the photon conversion efficiencies, capture and guiding efficiencies, transmission losses, and quantum efficiency of the SiPMs.

The magnetic coils, shown in Figs. 7 and 8, will be wires fixed onto a shell in the form of cosine θ coils. These coils provide the B_0 (horizontal and perpendicular to the long-axis of the cell), and RF-fields for spin-flipping and spin-dressing (horizontal and parallel to the long axis of the cell). Sheets of superconductors (not shown) will be used as a magnetic shield as well as shaping the flux return in order to achieve a high field uniformity.

To minimize operational costs of the cryostat there is an embedded cryocooler thermally linked to the main LHe bath, which significantly reduces LHe consumption. In addition, a 40 liters per day capacity He reliquefier was added to the system to recycle evaporated LHe. The recycled He is collected in the 250l storage Dewar, which in turn is connected to the cryostat by a custom designed transfer tube with a LN_2 precooling capability. As result, using LN_2 and cryocooler precooling we are able to reach about 15K temperature in the main bath and then start transfer LHe slowly from the storage Dewar minimizing need to replenish our helium inventory.

Appendix 3 MEASURING THE CORRELATION FUNCTION

A Measuring the correlation function of ^3He

The correlation function of ^3He , must be characterized prior to measuring the correlation function of the neutrons, as the signal from the neutrons is proportional to cosine of the angle from the ^3He . Therefore we only know the neutron's phase relative to the ^3He . The noise in the ^3He is due to noise in the SQUID, we will assume it is white noise.

1 Static Gradient method, T_1

There are three ways to access the correlation function through relaxation and frequency shifts. One of these is to measure the longitudinal relaxation with a constant gradient. After application of a constant gradient in the z direction such that $G_z = -2G_x = -2G_y$, we would measure the correlation function by the longitudinal relaxation rate due to the applied gradient. The contribution to the relaxation is given in [2, 8, 9].

Measuring the correlation function through the longitudinal relaxation is achieved with free induction decay (FID) decay and SQUIDs in the SOS apparatus. For this measurement we apply a known α pulse where $\alpha \ll \frac{\pi}{2}$. This forces the ^3He into a FID, which is measured by the SQUIDs. Once the decay (T_2^*) is below the noise we apply the relaxing gradient and wait for a given time. After the time has elapsed we supply another α pulse, measure the FID, and repeat. This measurement procedure continues for 5 to 6 T_1 time constants so the background is well known.

This measurement has a set of competing relaxation processes that are considered systematic effects, these effects can largely be corrected for with calibration measurements, within the precision of the corrections. The total longitudinal relaxation rate is given by the formula:

$$\frac{1}{T_{1,\text{tot}}} = \frac{1}{T_{1,\text{wall}}} + \frac{1}{T_{1,\text{gradient}}} + \frac{1}{T_{\text{pulse}}}, \quad (14)$$

where $T_{1,\text{wall}}$ is the relaxation for the cell walls, T_{pulse} is the loss from the α pulse, and $T_{1,\text{gradient}}$ is the quantity we are trying to measure. The precision of the measurement is given by:

$$\left(\frac{\sigma_{\text{gradient}}}{T_{1,\text{gradient}}}\right)^2 = \left(\frac{\sigma_{\text{measured}}}{T_{1,\text{tot}}}\right)^2 + \left(\frac{\sigma_{\text{wall}}}{T_{1,\text{wall}}}\right)^2 + \left(\frac{\sigma_{\text{pulse}}}{T_{\text{pulse}}}\right)^2 \quad (15)$$

Typically $T_{1,\text{gradient}}$ can be made much shorter than $T_{1,\text{wall}}$, and the error on the pulse loss and the wall relaxation can be made very small so the only contribution is the error of the gradient measurement. If this is not the case, the density of ^3He can be increased for a better calibration of the undesired relaxation, increasing density will increase signal without affecting the wall relaxation rate or the α pulse.

An appropriate choice for the gradient is $200 \mu\text{G cm}^{-1}$, and the relaxation rate as a function of holding field is shown in Fig. 9.

2 RF Gradient method, T_2

For the cell geometry T_2 relaxation in an RF gradient field:

$$\frac{1}{T_{2,\text{rf gradient}}} = \frac{\gamma^2 G_{zx}^2}{2} \text{Re}[S_{xx}(\omega_{rf})]. \quad (16)$$

Where G_{zx} represents a gradient in the z field along the x direction. We can account for other relaxation processes by the formula,

$$\frac{1}{T_{2,\text{tot}}} = \frac{1}{T_{2,\text{wall}}} + \frac{1}{T_{2,\text{rf gradient}}}. \quad (17)$$

Notice the absence of the T_{pulse} term, this is because we apply a $\frac{\pi}{2}$ pulse at the start of the measurement. The $\frac{\pi}{2}$ pulse must be well known to provide maximum signal strength, but it no longer requires a correction to the measurement. To measure $T_{2,\text{tot}}$ we first apply the $\frac{\pi}{2}$ pulse, record the FID decay with the SQUIDs for a given time interval long enough to give a good SNR. When this measurement period is over we turn off the SQUIDs, apply an RF gradient for a given time period, turn off the RF gradient, measure the signal,

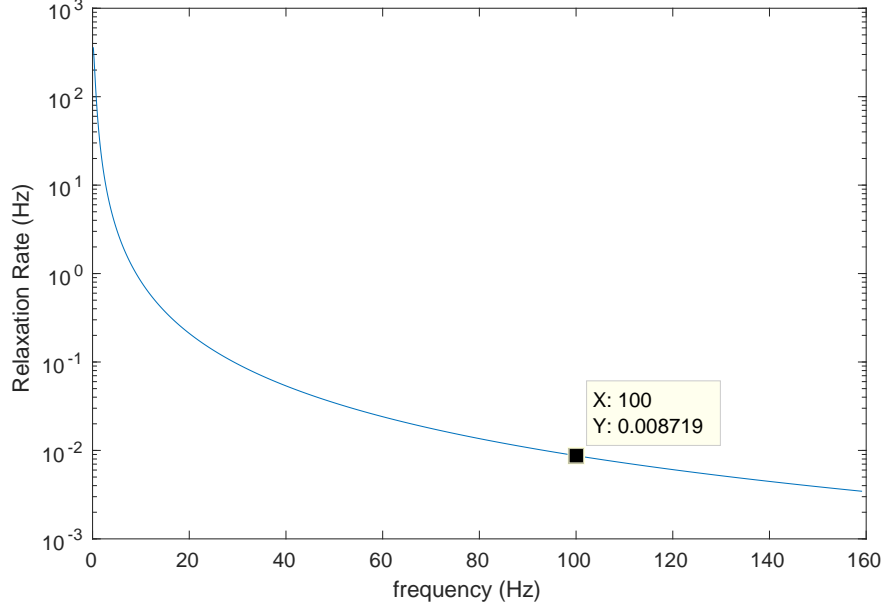


FIG. 9. Plot of the longitudinal relaxation rate (or transverse with an RF gradient) rate of ^3He in a $200\ \mu\text{G cm}^{-1}$ gradient along the 40 cm cell direction.

and repeat until for 5-6 $T_{2,\text{tot}}$ time constants for a good background measurement. The errors propagate as,

$$\left(\frac{\sigma_{\text{rf gradient}}}{T_{2,\text{rf gradient}}}\right)^2 = \left(\frac{\sigma_{\text{measured}}}{T_{2,\text{tot}}}\right)^2 + \left(\frac{\sigma_{\text{wall}}}{T_{2,\text{wall}}}\right)^2. \quad (18)$$

because there is no systematic effect from errors in the pulse calibration this method is preferred over T_1 , however it may take effort in tuning the RF gradient.

3 Measuring the B^2 shift

A very promising option is to measure the B^2 shift. Given by the formula [9],

$$\delta\omega_{B^2} = \frac{\gamma^2}{2} (G_x^2 \text{Im}[S_{xx}(\omega)] + G_y^2 \text{Im}[S_{yy}(\omega)]). \quad (19)$$

This is attractive because it is a direct measure of the imaginary component of the correlation function. While it may be challenging, in principle we can apply a gradient to excite the shift (shift gradient) along B_x in x and an opposing gradient in B_y in y , leaving a uniform field in the B_z so that T_2 remains long. The shift will be dominated by the gradient in the cell's long dimension. When the shift gradients are energized the holding field will change slightly due to offsets in shift coils and the cell position, it will appear as a frequency shift. This can be accounted for by measuring the frequency with the shift gradient turned off (measuring ω_0) and measurements with the shift gradient reversed ($\omega_{\pm I}$). The B^2 shift can be determined by,

$$\delta\omega_{B^2} = \frac{\omega_{+I} + \omega_{-I}}{2} - \omega_0. \quad (20)$$

The sensitivity of the measurement is determined from the signal to noise ratio (SNR) at the maximum in

the Fourier transform, T_2 , and the measurement time T , written in terms of T_2 , $T = \alpha T_2$.

$$\sigma_{\delta\omega_{B^2}} = \frac{1}{\text{SNR}} \frac{1}{T_2} \frac{1}{1 - (\alpha + 1)e^{-\alpha}} \quad (21)$$

With $\alpha = 5$ we achieve 96% of the total sensitivity. This implies a measurement time of $T \approx 5000$ s, and translates to a frequency resolution of $\Delta f \approx 2 \times 10^{-4}$ Hz. However, according to the sampling theorem, when T is chosen such that the remainder of the signal is negligible, the frequency resolution can be made arbitrarily small, without distortion, by zero padding the time discrete Fourier transform, with time samples short enough to avoid aliasing.

To estimate the sensitivity in frequency if we assume a $T_2 \approx 400$ s and the time signal, $S(t)$ at the start of the measurement is one tenth the RMS noise then the signal to noise ratio,

$$\text{SNR} = T_2 \frac{S(0)}{\sigma_S} = 40, \quad (22)$$

and we have a sensitivity of $\sigma_{\delta\omega_{B^2}} \approx 6.25 \times 10^{-5} \frac{\text{rad}}{\text{s}}$ or $\sigma_{\delta f_{B^2}} \approx 9.94 \times 10^{-6}$ Hz. In this scenario if a shift gradient of $10 \frac{\mu\text{G}}{\text{cm}}$ is applied, the imaginary part of the correlation function could be determined to around 1% in a single measurement. This is shown in Fig. 3.

B Measuring the correlation function of neutrons

Because the neutron density is on the order of 10^{-10} smaller than ^3He they cannot be read out by the SQUIDS. The spin dependent interaction with ^3He will allow measurements of the neutron correlation function. The neutron correlation function can be measured in a similar way to the ^3He by measuring the relaxation in a known gradient. Here we go over the implications of both the T_1 , T_2 and $\delta\omega_{B^2}$ methods.

1 Longitudinal Relaxation (T_1) with static gradient

Similar to ^3He , measurement of the longitudinal relaxation of the UCNs can be accomplished by repeatedly tipping the spins by a known small angle α , with a given time interval between FID signals to measure the decay. The gradient must be turned off during FID to allow maximum T_2 and therefore signal strength. The overall decay (measured decay) of the polarization can be written as a sum of rates,

$$\frac{1}{T_1} = \frac{1}{\tau_{\text{bottle}}} + \frac{1}{T_{1,\text{gradient}}} + \frac{1}{T_{\text{pulse}}} + \frac{1}{\tau_3} + \frac{1}{T_{1,^3\text{He}}} \quad (23)$$

Where $T_{1,\text{gradient}}$ is the time constant of interest, and all other terms are systematic errors. Where τ_{bottle} is a combination of the neutron lifetime in the cell and the neutron wall depolarization time, T_{pulse} is the loss from tipping pulses required to measure the FID signal, and τ_3 is the rate the neutrons are lost during the measurement from the spin dependent cross section, $T_{1,^3\text{He}}$ is the relaxation of the ^3He . Good precision and will be needed to minimize the error of the $T_{1,\text{gradient}}$ and it will need several dedicated measurements to account for systematic errors on the measurement of $T_{1,\text{gradient}}$, presumably $T_{1,^3\text{He}}$ would already be known fairly well due to measurements of the ^3He correlation function. Furthermore it can be made such that $T_{1,\text{gradient}}$ is much shorter than the other time constants, thus reducing the impact of systematic errors, except T_{pulse} . Errors of this relaxation process propagate like

$$\left(\frac{\sigma_{\text{gradient}}}{T_{1,\text{gradient}}} \right)^2 = \left(\frac{\sigma_{\text{measured}}}{T_1} \right)^2 + \left(\frac{\sigma_{\text{bottle}}}{\tau_{\text{bottle}}} \right)^2 + \left(\frac{\sigma_{\text{pulse}}}{T_{\text{pulse}}} \right)^2 + \left(\frac{\sigma_{\tau_3}}{\tau_3} \right)^2 + \left(\frac{\sigma_{T_{1,^3\text{He}}}}{T_{1,^3\text{He}}} \right)^2 \quad (24)$$

We see that the measurement of the neutron correlation function will require much more calibration and has more sources of error. This may require more measurements for improved statistics, but if all the other

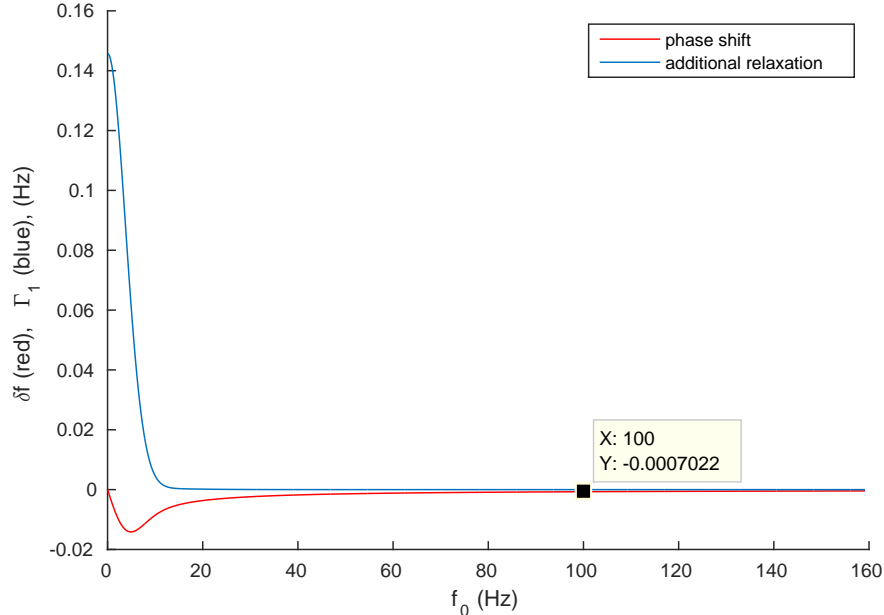


FIG. 10. Plot of the B^2 shift of neutrons in a $10 \mu\text{G cm}^{-1}$ gradient along the 40 cm cell direction

sources of error are well characterized a single measurement with a starting S/N of 100 would be required.

2 Transverse Relaxation (T_2) with RF gradient

Another method to measure the correlation function would be to apply a $\frac{\pi}{2}$ pulse to the ^3He and the neutrons and watch the FID decay from the scintillations of the spin dependent cross-section. Again, as with ^3He this method is attractive because it eliminates the pulse loss systematic error, typically the largest source of error for T_1 measurements. For T_2 we have,

$$\frac{1}{T_2} = \frac{1}{\tau_{\text{bottle}}} + \frac{1}{T_{2,\text{rf gradient}}} + \frac{1}{T_{n,^3\text{He}}} + \frac{1}{T_{2,^3\text{He}}} \quad (25)$$

As the spins decay the oscillating signal from the spin-dependent cross section becomes a constant background signal. The total integrated background and signal can be used as a normalization. $T_{2,^3\text{He}}$, is the relaxation of ^3He , this can be directly calculated from the correlation function measured during the ^3He measurements. Errors would propagate like the previous cases.

3 Measuring the B^2 shift of neutrons

Unlike the case for ^3He , when we are measuring neutrons we are directly measuring the relative phase of the neutrons to the ^3He . It should be possible to measure the frequency shift due to the additional B field gradients. This possibility is shown in the Fig. 10, and where it is seen with $10 \mu\text{G/cm}$ gradient we find a shift of 7×10^{-4} Hz, easily detectable in the SOS apparatus.

Regardless of the ability to measure this shift I suspect it will be an important exercise, it is very attractive because it is a direct measurement of the imaginary part of the correlation function. There would be no model dependence. Furthermore this would be testing the measurement of a frequency shift, and could provide critical experience in measuring frequency shifts of UCN- ^3He samples in an agile apparatus.

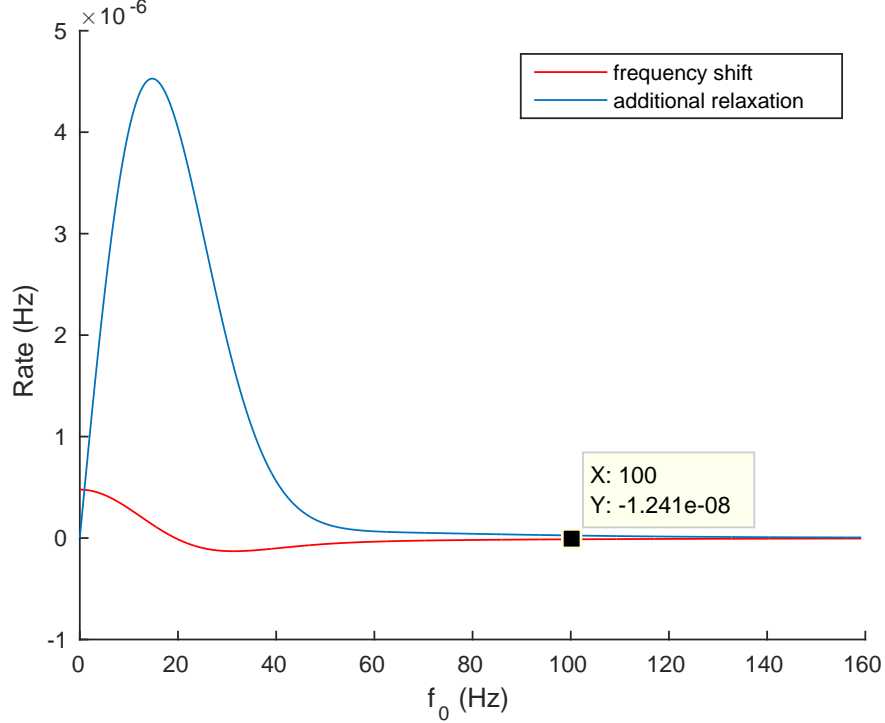


FIG. 11. Plot of the linear-in-E frequency shift of neutrons in a E-field of 75 kV cm^{-1} and a $10 \mu\text{G cm}^{-1}$ gradient field along the 40 cm cell direction

C Conclusion on correlation function measurements

In principle the SNS nEDM apparatus can make all the measurements that the SOS apparatus can make. For ^3He it must use the same techniques to measure the correlation function. However for UCNs there is a choice: either use correlation function or it can directly measure the false frequency shift (see Eq. 2), by applying a $10 \mu\text{G/cm}$ gradient in presence of an E field (such gradient will raise the false frequency shift while keeping T_2 long enough for an adequate measurement). The numerical values of the measured effects for this two cases can be seen on figure 11 (neutron false EDM) and figure 10 (neutron false EDM).

One can see that for the same gradient, the false edm frequency shift, $\delta\omega_{\text{EB}}$, is 10^{-4} times smaller than the $\delta\omega_{B^2}$, making it more difficult to measure precisely. Furthermore it suffers from the same problem as the B^2 shift in that the coils must be centered to good precision. There will be additional systematic frequency shifts due an offset in the B_0 and gradient field coils, it will be distinguishable from $\delta\omega_{\text{EB}}$ by reversing the B gradient fields.

Appendix 4 MEASURING NEUTRON LONGITUDINAL RELAXATION TIME $T_{1,n}$

As mentioned in Sec. III C, the neutron longitudinal relaxation time $T_{1,n}$ can be measured by observing the scintillation light when leaving both the neutron and ^3He spins aligned with B_0 . Here we are discussing the case of no applied magnetic field gradients. In this case, the angle between the ^3He and neutron polarizations is zero, and thus the scintillation light is given by Eq. 10 with $\phi(t) = \omega_{\text{free}}t_i + \phi_0 = 0$ and replacing $T_{2,\text{tot}}$ with $T_{1,\text{tot}}$, where $T_{1,\text{tot}}^{-1} = T_{1,n,\text{walls}}^{-1} + T_{1,^3\text{He},\text{walls}}^{-1}$ (since the $T_{1,\text{gradients}}$ for the neutron and ^3He are extremely

long). That is, we expect the light signal to be:

$$\frac{y(t_i)}{\Delta t} = I_0 e^{-t_i/\tau_{\text{tot}}} \left[1 - F e^{-t_i(T_{1,n,\text{walls}}^{-1} + T_{1,^3\text{He,walls}}^{-1})} \right] + R_{\text{BG}} \quad (26)$$

$$= I_0 e^{-t_i/\tau_{\text{tot}}} - I_0 F e^{-t_i(\tau_{\text{tot}}^{-1} + T_{1,n,\text{walls}}^{-1} + T_{1,^3\text{He,walls}}^{-1})} + R_{\text{BG}} \quad (27)$$

$$= N_0 \frac{\epsilon_3}{\tau_3} \left[\left(\frac{\epsilon_\beta \tau_3}{\tau_\beta \epsilon_3} + 1 \right) e^{-t_i/\tau_{\text{tot}}} - P_3 P_n e^{-t_i(\tau_{\text{tot}}^{-1} + T_{1,n,\text{walls}}^{-1} + T_{1,^3\text{He,walls}}^{-1})} \right] + R_{\text{BG}} . \quad (28)$$

This is a sum of two exponential decays with different time constants. As mentioned in Sec. III C, τ_{walls} and $T_{1,^3\text{He,walls}}$ will be determined independently with different measurements. Fitting for the two time constants, and scanning the x_3 used, should allow $T_{1,^3\text{He,walls}}$ to be determined.

-
- [1] M. Ahmed, R. Alarcon, A. Aleksandrova, S. Baeßler, L. Barron-Palos, L. Bartoszek, D. Beck, M. Behzadipour, I. Berkutov, J. Bessuille, *et al.*, *Journal of Instrumentation* **14**, P11017 (2019).
 - [2] A. Redfield, *IBM Journal* **January**, 19 (1957).
 - [3] S. K. Lamoreaux and R. Golub, *Phys. Rev. A* **71**, 032104 (2005).
 - [4] Guillaume Pignol, Stephanie Roccia, *Physical Review A* **84**, 042105(5) (2012).
 - [5] C. M. Swank, A. K. Petukhov, and R. Golub, *Phys. Rev. A* **93**, 062703 (2016).
 - [6] Riccardo Schmid, *New search for the Neutron Electric Dipole Moment using Ultracold Neutrons at the Spallation Neutron Source*, Ph.D. thesis, California Institute of Technology (2013).
 - [7] Christopher Swank, *An Investigation in the Dynamics of Polarized Helium-3 in Superfluid Helium-4 for the Spallation Neutron Source (SNS) neutron-electric-dipole-moment (nEDM) experiment.*, Ph.D. thesis, North Carolina State University (2012).
 - [8] D. D. McGregor, *Physical Review A* **45**, 2631 (1990).
 - [9] G. Pignol, M. Guigue, A. Petukhov, and R. Golub, *Physical Review A* **92**, 053407 (2015).